NOTCH STRENGTH OF SINTERED TUNGSTEN ALLOYS

S. KOBAYASHI, Y. MUTOH* and Y. HOSOKAI*
Department of Mechanical Engineering, Nagaoka College of Technology, Nishi-katakai, Nagaoka-shi, 940 Japan
**Department of Mechanical Engineering, Nagaoka University of Technology, Kamitomioka, Nagaoka-shi, 940-21 Japan*

ABSTRACT

Fracture strength and fracture behavior of sintered two-phase tungsten alloy specimens with various notch root radii were investigated. Cracks mainly initiated by interface decohesion between tungsten particles at the notch root. Cleaveage fracture of tungsten particle also became found with increasing the volume fraction of ductile matrix phase. No significant variation of crack initiation strength was found for the radii larger than 5mm. However, crack initiation strength significantly decreased with reducing notch radius for the radii smaller than 5mm. The non-linear notch mechanics proposed by Nisitani et al has been successfully applied to the present materials.

KEYWORDS

Notch strength, Crack initiation, Tungsten alloy, Non-linear notch mechanics.

INTRODUCTION

Sintered tungsten alloy W-Ni-Fe is produced by liquid-phase sintering technique and has two phases : ductile Ni-Fe matrix and hard W particle. This alloy was originally developed for a radiation shelter material. However, due to its excellent properties such as high strength at elevated temperatures, corrosion resistance, and wear resistance, application of this alloy to structural components becomes wider. Under these circumstances a lot of research works have been reported, such as effects of heat-treatment (Yoon et al, 1983, Kaneko and Amano, 1988) , impurity (Ekbom, 1976, Edmonds and Jones, 1978, Eisenmann and Geraman, 1982) and temperature (O'Donnell and Woodward, 1990, O'Donnell et al, 1992) on mechanical properties. The authors have also reported several research works : impact strength (Kobayashi et al, 1990) , effects of tungsten content and strain rate on mechanical properties (Kobayashi et al, 1992) , effects of tungsten content and loading rate on fracture toughness (Kobayashi et al, 1993) and high temperature tensile strength (Kobayashi et al, 1996) . These reports reveal complicated but interesting phenomena that in tensile tests, cleavage fracture of tungsten particles becomes dominant with an increase in ductility, and in fracture toughness tests, interface decohesion of tungsten and ductile fracture of matrix phase become dominant with an increase in toughness. Notch strength is obviously essential for designing structural component with arbitrary shape. However, no report on notch strength and fracture behavior of sintered tungsten alloys is available.

In the present study, fracture processes of notch specimens with various root radii ranging from 1mm to 100mm have been observed in detail using two tungsten alloys with different tungsten content. Effects of root radius and tungsten content on notch strength have been discussed. The material characteristic value for notch, that is the relationship between maximum equivalent plastic strain and notch root radius, based on the non-linear notch mechanics (Nisitani et al, 1995) , has been also evaluated.

EXPERIMENTAL PROCEDURE

The materials used are two sintered tungsten alloys with different tungsten content. The compositions of source powders are shown in Table 1. The higher tungsten content material is named the material A and the lower one is named the material B. It is known that the best properties of Ni-Fe matrix can be achieved when the ratio of Ni and Fe is 7 : 3. The present materials also have the same Ni-Fe ratio. After mixture and compaction of source powders, primary sintering at 1300℃ for 1.5h and then secondary sintering at 1475℃ for 1.5h were conducted. The mechanical properties and microstructures of the materials used are shown in Table 2 and Fig. 1, respectively. Contact between tungsten particles was dominant in the material A with higher tungsten content. Tungsten particles were surrounded with Ni-Fe matrix phase in the material B, while contacts between tungsten particles were also found to some extent.

Specimens with dimensions of 10 × 10 × 55 (mm) were machined and 2mm deep notch with various root radii ranged from 1mm to 100mm were introduced at the center of the specimens. 3mm and 4mm deep notches with root radius of 2mm were also introduced to confirm the effectiveness of the non-linear notch mechanics. Notch root surfaces were polished by using alimina slurry to observe crack initiation and growth. Three-point bend test with span length of 40mm and crosshead speed of 0.5mm/min was carried out on an Instron type universal test machine.

Table 1 Composition, density and volume fraction of W-particle for the material used

	Composition of powder (wt%)			Density (Mg/m^3)	Volume fraction (%)	
	W	Ni	Fe		W	Matrix
A	97.2	2.0	0.8	18.6	93.0	7.0
B	93.0	4.9	2.1	17.7	83.2	16.8

Table 2 Mechanical properties of the material used

		A	B
Young's modulus E	(GPa)	380	321
0.2% Proof stress $\sigma_{0.2}$	(MPa)	695	648
Tensile strength σ_B	(MPa)	938	935
Elongation	(%)	13.9	34.5

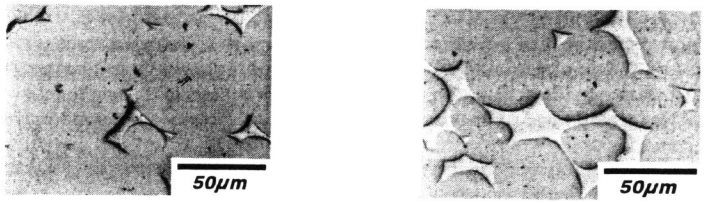

(a)Material A (b)Material B

Fig.1 Micrographs of the materials used

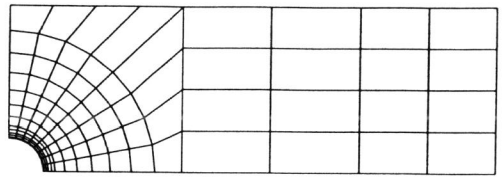

Fig.2 Finite element model

The test was interrupted at certain load levels to observe the crack initiation and propagation processes at the notch root by a scanning electron microscope (SEM) .

FINITE ELEMENT ANALYSIS

In order to investigate a condition for crack initiation based on the present observations, stress and strain distributions near notch root were analyzed by using the finite element method (FEM) . The universal FEM code MARC was utilized for elastic-plastic finite element analysis. An example of finite element model is illustrated in Fig.2. The sizes of three elements beneath notch root were similar, namely 40 μ m, which was almost equal to the tungsten particle size, regardless of notch root radius. The plain-strain eight-node isoparametric elements were used. The true stress-true strain relations for the materials A and B were used for the material constitutive equations (Kobayashi et al, 1990) .

RESULTS AND DISCUSSION

Observations of crack initiation

Initiated cracks at notch root for the materials A and B with root radii of 2mm and 100mm are shown in Figs. 3 and 4, respectively. In the case of the material A, due to low volume fraction of Ni-Fe matrix phase, cracks initiated and coalesced to grow by decohesion of interface between

tungsten particles without large deformation. In the case of the material B, cracks initiated dominantly by decohesion of interface between tungsten particles. However, cracks also initiated by cleavage fracture of tungsten particle, which were observed in the tensile specimens (Kobayashi et al, 1992) , as shown in Fig.4 (b) . Tungsten particles surrounded with ductile matrix phase, so that they were deformed rather freely and a lot of traces of slip were observed in the tungsten particles.

Crack initiation load

The relationships between crack length measured on the SEM observations and load for the materials A and B are shown in Figs. 5 and 6, respectively. As can be seen from the figures, cracks initiated and propagated at lower load for smaller root radius (sharper notch) . The load of crack initiation and growth for the material B with high ductility was high compared to the material A. The crack initiation load was defined as the load at which the relationship between crack length and load, shown in Figs.5 and 6, was extrapolated to the point of zero crack length. Figure 7 shows the relationship between the crack initiation load estimated and notch root radius.

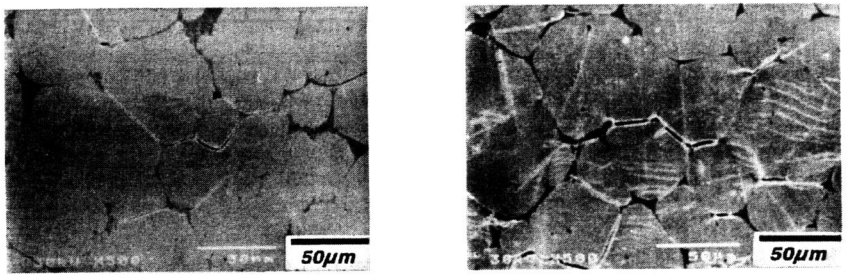

(a)R=2mm (b)R=100mm

Fig.3 Initiated cracks (Material A)

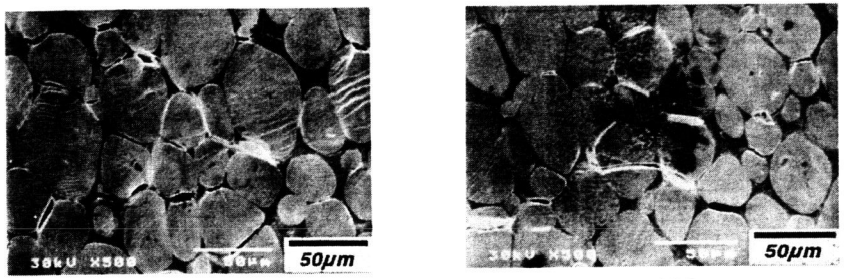

(a)R=2mm (b)R=100mm

Fig.4 Initiated cracks (Material B)

As can be seen from the figure, the crack initiation load is significantly influenced by notch root radius in the region of notch root radii smaller than 5mm : the crack initiation load significantly decreased with reducing notch root radius. However, gradual variation of the crack initiation load is observed for notch root radii larger than 5mm. Therefore, in the design of structural components containing notch-like features, it is effective to make notch root radus larger than 5mm from the safty point of view.

Fracture surface morphology

Fractographs near notch root of the materials A and B are shown in Fig.8. For the material A, as shown in Fig.8 (a) , fracture surfaces caused by interfacial decohesion between tungsten particles were dominant regardless of notch root radius, while cleavage fracture of tungsten particle was very locallized. For the material B, mixed fracture surfaces of interfacial decohesion between tungsten particles and transgranular cleavage fracture of tungsten particle were observed. Higher area fraction of cleavage fracture in the material B compared to the material A results from higher content of ductile matrix phase and large deformation for crack initiation and growth (Kobayashi et al, 1992) . These fracture surface morphologies are obviously different from the case of fracture toughness specimen, where a crack initiates from a sharp precrack and propagation is transgranular by cleavage mode for the material A, and through the matrix phase by ductile fracture mode for the material B (Kobayashi et al, 1993) . On the other hand, the modes observed in notched specimens resemble those for fractured tensile specimens (Kobayashi et al, 1992) .

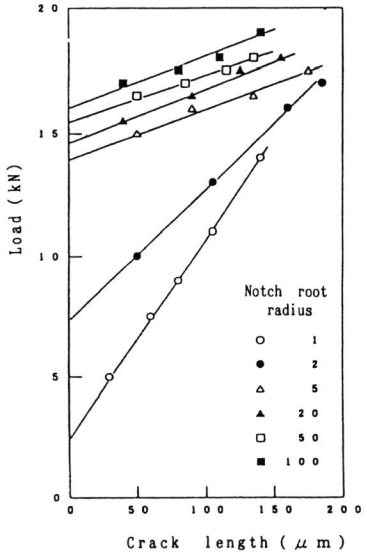

Fig.5 Relationship between load and crack length (Material A)

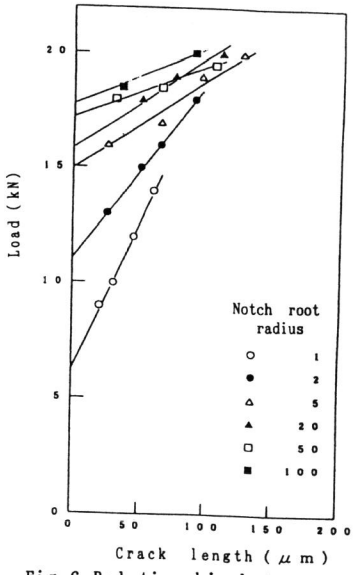

Fig.6 Relationship between load and crack length (Material B)

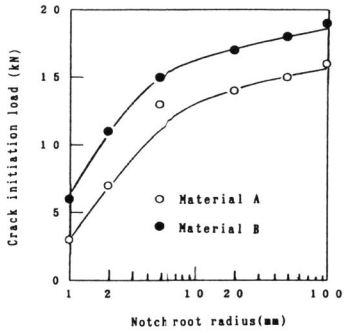

Fig.7 Relationship between crack initiation load and notch root radius

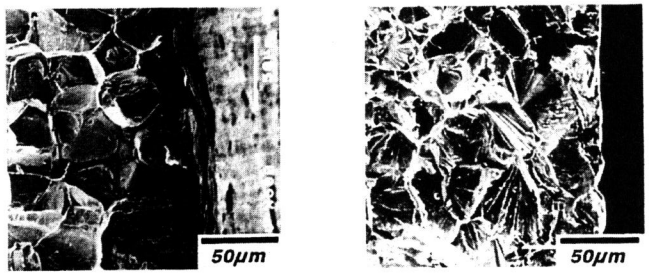

(a)Material A (b)Material B

Fig.8 Fractographs near notch root

Discussion on the non-linear notch mechanics

Nisitani et al, (1994) , have proposed the non-linear notch mechanics, which is applicable to large scale yielding condition, by expanding the linear notch mechanics (Nisitani, 1983, 1987) . According to the non-linear notch mechanics, when both the maximum equivalent plastic strains at notch root and the notch root radii of two bodies coincide, stress and strain fields near the notch root of the two bodies are identical and independent of notch depth and ligament width. Therefore, the relationship between maximum equivalent plastic strain at fracture and notch root radius gives a fracture criterion for the material concerned, which corresponds to ,for example, the material characteristic value K_{IC} in the linear fracture mechanics. Therefore, the material characteristic relationship based on the non-linear notch mechanics enables one to design structural components containing notch-like features. In this section, the effectiveness of the non-linear notch mechanics is confirmed for the present materials, and the material characteristic relationships between maximum equivalent plastic strain at crack initiation and notch root radius for the present tungsten alloys is evaluated.

The relationships between crack length and load for the material B with notch root radius of 2mm and notch depths of 2, 3 and 4mm are shown in Fig.9. The stress-strain distributions near the notch root at the crack initiation loads determined from the figure were estimated by elastic-plastic finite element analysis. From the results, the equivalent plastic strain distributions are shown in Fig.10. As can be seen from the figure, the equivalent plastic strain distributions and also the maximum equivalent plastic strains at crack initiation coincide regardless of notch depth. Although we have omitted the indication of distributions of other stresses and strains, they also coincided regardless of notch depth. Thus, the non-linear notch mechanics was confirmed to be applicable to the present material.

For the specimens plotted in Fig.7, the distributions of equivalent plastic strain at crack initiation load were estimated based on the elastic-plastic finite element analysis.The result for Material B is shown in Fig.11. From these results, the relationships between the maximum equivalent plastic strain at crack initiation and notch root radius are shown in Fig.12. These curves indicate the material characteristics for crack initiation at a notch root. Therefore, safety and reliability for fracture of practical components with notch-like features can be evaluated by combining the crack initiation criterion shown in Fig.12 and the result of finite element analysis of the notched components, where sizes of elements beneath notch root should coincide with those in the present finite element models : 40 μm for the nearest three elements.

CONCLUSIONS

Fracture behavior of notched specimens with various notch root radii from 1mm to 100mm were investigated in sintered tungsten alloys with two different tungsten contents. Main conclusions obtained are summarized as follows.

(1) Although cracks initiated at the notch root by interfacial decohesion between tungsten particles, crack initiation by transgranular cleavage fracture was increasingly observed with increasing

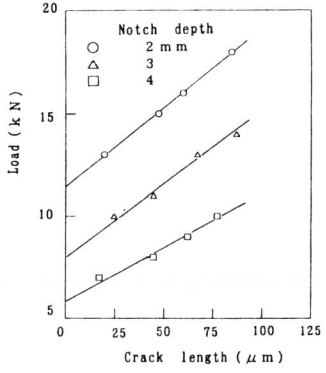

Fig.9 Relationship between load and crack length (Material B, R=2)

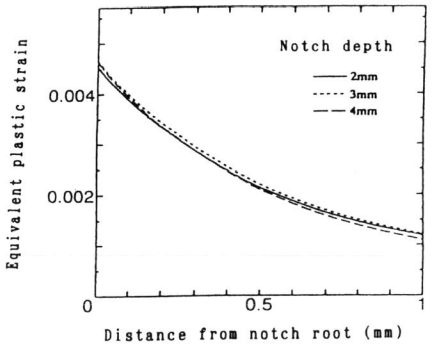

Fig.10 Strain distributions (Material B, R=2)

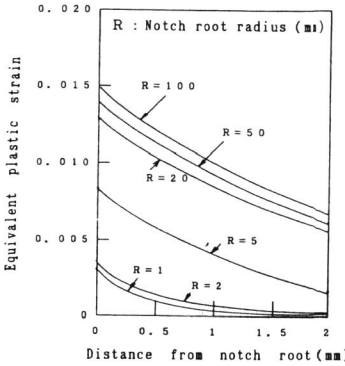

Fig.11 Strain distributions (Material B, Notch depth 2mm)

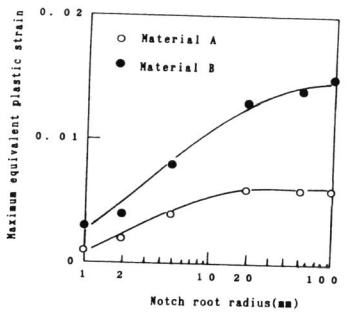

Fig. 12 Relationship between maximum equivalent plastic strain and notch root radius

matrix phase content.

(2) The crack initiation load was significantly influenced by notch root radius for the radii smaller than 5mm : the crack initiation load rapidly decreased with reducinig notch root radius. On the other hand, effect of notch root radius was not significant for the radii larger than 5mm.

(3) The non-linear notch mechanics proposed by Nisitani et al was applicable to the present material. The relationship between maximum equivalent plastic strain at fracture and notch root radius, which is the material parameter to give a fracture criterion, was determined for the present two kinds of sintered tungsten alloy by combining the experiments with finite element analysis.

REFERENCES

Edmonds, D. V. and P. N. Jones (1979). *Metall. Trans.*, **10A**, 289-295.
Eisenmann, M. R. and R. M. German (1982). *Prog. Powder Met.*, **38**, 203-213.
Ekbom, L. (1976). *Scan. J. Metall.*, **5**, 179-184.
Kaneko, T. and Y. Amano (1988). *J. of Jpn. Soc. Powder and Powder Metall.*, **35**, 558-562.
Kobayashi, S., M. Nakayama, Y. Mutoh and K. Tanaka (1990). *Trans. Jpn. Soc. Mech. Eng.*, **56**, 2070-2077.
Kobayashi, S., K. Ichikawa, Y. Mutoh and T. Satoh (1992). *J. of Soc. of Mater. Sci., Jpn.*, **41**, 1088-1094.
Kobayashi, S., K. Ichikawa and Y. Mutoh (1993). *J. of Soc. of Mater. Sci., Jpn.*, **42**, 555-560.
Kobayashi, S., Y. Mutoh, Y. Hosokai, S. Iwata and S. Mizuno (1996). *J. of Soc. of Mater. Sci., Jpn.*, **45**, 183-188.
Nisitani, H. (1983). *Trans. Jpn. Soc. Mech. Eng.*, **48**, 1353-1359.
Nisitani, H. (1987). In: *Role of Fracture Mechanics in Modern Technology* (G.C.Sih, H.Nisitani, T.Ishihara, ed.), pp.25-37. Elsevier Science Publ. B.V. Amsterdam.
Nisitani, H. and W. Fujisaki. (1994). *Trans. Jpn. Sci. Mech. Eng.*, **60**, 2525-2531.
O'Donnell, R. G. and R. L. Woodward (1990). *Metall. Trans.*, **21A**, 744-748.
O'Donnell, R. G., S. J. Alkemade and R. L. Woodward (1992). *J. Mater. Sci.*, **27**, 6490-6494.
Yoon, H. K., S. H. Lee, S. J. L. Kang and D. N. Yoon (1983). *J. Mater. Sci.*, **18**, 1374-1380.